Research Square

Preprints are preliminary reports that have not undergone peer review.
They should not be considered conclusive, used to inform clinical practice,
or referenced by the media as validated information.

Celastrol can inhibit the growth of SHH medulloblastoma: In vitro and in vivo studies

[redacted]
The Second Affiliated Hospital and Yuying Children's Hospital of Wenzhou Medical University
[redacted]
The Second Affiliated Hospital and Yuying Children's Hospital of Wenzhou Medical University
[redacted]
The Second Affiliated Hospital and Yuying Children's Hospital of Wenzhou Medical University
[redacted]
Zhoushan Woman and Children Hospital
[redacted]
The Second Affiliated Hospital and Yuying Children's Hospital of Wenzhou Medical University
[redacted]
The Second Affiliated Hospital and Yuying Children's Hospital of Wenzhou Medical University
[redacted]
The Second Affiliated Hospital and Yuying Children's Hospital of Wenzhou Medical University
[redacted]
The Second Affiliated Hospital and Yuying Children's Hospital of Wenzhou Medical University
[redacted]
The Second Affiliated Hospital and Yuying Children's Hospital of Wenzhou Medical University
[redacted] (13806882921@163.com)
The Second Affiliated Hospital and Yuying Children's Hospital of Wenzhou Medical University

Research Article

Keywords: medulloblastoma, celastrol, ROS, anticancer

Posted Date: January 8th, 2024

DOI: https://doi.org/10.21203/rs.3.rs-3836653/v1

License: This work is licensed under a Creative Commons Attribution 4.0 International License.
Read Full License

Additional Declarations: No competing interests reported.

Abstract

Celastrol is a naturally occurring compound with a range of pharmacological properties derived from the traditional Chinese herb *Tripterygium wilfordii*. To develop a new therapeutic strategy for medulloblastoma (MB), this study will investigate the inhibitory effect of celastrol on MB and its underlying signaling pathway. We evaluated the effects of celastrol on cell proliferation using the CCK-8 assay and colony formation assay. Scratch assays and transwell invasion assays were used to assess the effects of celastrol on metastasis. The flow cytometry method was used to detect apoptosis and reactive oxygen species (ROS) levels in the cells. The potential signaling pathways were detected by transcriptomics and quantitative PCR. To study the anticancer effect of celastrol on MB in vivo using a mouse xenograft model. Cell proliferation and metastasis of the SHH subgroup MB cell line can be inhibited by celastrol, and the effect of the drug on apoptosis is associated with its proliferation inhibition effect. Animal experiments showed that celastrol inhibited the growth of MB in vivo. In addition, the pro-apoptotic effect of celastrol on ONS-76 cells may be caused by ROS. Our findings indicate that celastrol inhibits the progression of MB both in vitro and in vivo, and this effect is associated with the induction of ROS in cells by celastrol in vitro studies.

Introduction

In children, MB is the most common malignant brain tumor[1]. Three molecular subgroups of MB can be identified: WNT, SHH, and non-WNT/non-SHH[2]. WNT-MB is found in the embryonic lower rhombic lip (LRL), whereas Sonic Hedgehog (SHH)-driven medulloblastoma (SHH-MB) and non-WNT/non-SHH MB are found in the cerebellar precursor matrix[3]. The MB is primarily treated with surgical resection, radiotherapy, and chemotherapy as adjuvant therapy[4]. However, treatment outcomes are often suboptimal, leading to severe long-term side effects[3].

Approximately 30% of MBs are SHH subtypes and are frequently diagnosed in infants and adults[5]. One or more genes of the SHH pathway are usually mutated in the SHH subgroup[6]. A two-class approach to inhibiting SHH has been developed: upstream antagonists of Smoothened (SMO) receptors and downstream inhibitors of GLI transcription factors[7]. Unfortunately, it is associated with a poor prognosis and often leads to drug resistance[8]. With many MB patients still facing challenges in achieving disease control, there is an urgent need to uncover novel targets for developing more precise, safe, and effective anticancer medications.

Autophagy, a lysosomal degradation system of cytoplasmic components, contributes to cellular homeostasis through the turnover of various biomolecules and organelles, often selectively[9]. Autophagy exhibits a dual role in shaping the development and progression of cancer, exerting both promoting and inhibiting effects depending on the tumor's stage and type[10]. But even so, recent studies have demonstrated that autophagy can eliminate drug-resistant tumors[11]. During the process of autophagy regulation, the AMPK pathway takes the lead in initiating autophagy and orchestrating autophagosome formation through phosphorylation of specific targets[12]. As an evolutionarily conserved

serine/threonine protein kinase, AMPK functions as a cellular energy sensor and governs an array of metabolic processes, including those pertinent to cancer[13]. Currently, AMPK is well known as an effective target for anticancer treatments[14].

Apart from authophagy, the ubiquitin-proteasome system (UPS) serves as another pivotal cellular homeostasis mechanism, essential for maintaining cellular balance, orchestrating signal transduction, and determining cell destinies[15]. Considering the higher rates of protein turnover in cancer cells, their increased reliance on the UPS renders it an attractive target for inhibition through targeted therapeutic approaches[16].

Therefore, we screened some compounds in the library consisting of inhibitors targeting autophagy and UPS pathways, and celastrol was one of these compounds. We determined the IC50 value of celastrol for MB and found the inhibitory effect of celastrol on the proliferation and migration of MB, which provides a new method for the treatment of MB. This study also expands the understanding of the mechanism of action of celastrol in MB and provides clues for the subsequent development of celastrol drugs.

Result

Celastrol was identified through drug screening

Screening of the top 50 drugs from the ubiquitin and autophagy drug libraries was performed at a concentration of 10 μM (Fig. 1A). The drugs obtained from the screening were further assessed for their half maximal inhibitory concentrations (IC50 concentrations), yielding an IC50 value of 2.102 (1.91–2.293) (Fig. 1B). Therefore, the subsequent experiments were performed exclusively with celastrol at a concentration of 2 μM, unless specified otherwise.

Celastrol has the capacity to influence the proliferation of SHH subtype medulloblastoma

To validate the anticancer potential of celastrol in SHH subtype MB, we performed a CCK-8 assay to measure cell viability. Upon exposure of ONS-76 cells to 2 μM of celastrol for varying durations (0, 1, 2, 3, 4, and 5 days), we observed a progressive decrease in cell viability with increasing treatment duration (Fig. 1C). Additionally, the results of the colony formation assay revealed a progressive reduction in both the number and size of colonies following celastrol treatment (Fig. 1D, E).

Celastrol can inhibit the invasion and migration of medulloblastoma cells

To evaluate the impact of celastrol on MB dissemination, we conducted transwell assays to test the effect of celastrol on MB migration and invasion. We found the ability of cells to migration (Fig. 2A, B) and invasion (Fig. 2C,D) significantly reduced upon celastrol treatment. To validate the results of transwell assays, we carried out the cell scratch assays and observed a remarkably reduced migration of

cells (Fig. 2E and F). Taken together, these results indicated that celastrol exhibits significant efficacy in suppressing the invasion and migration of SHH-MB.

Celastrol can induce cell apoptosis via upregulation of ROS levels.

To further investigate the potential mechanism by which celastrol inhibits SHH-MB, we performed the flow cytometry analysis to assess the impact of celastrol on ONS-76 cell apoptosis (Fig. 3A). The flow cytometry results revealed a significantly higher percentage of apoptotic ONS-76 cells following 24-hour treatment with celastrol, compared to the DMSO control group (Fig. 3B).

To ascertain the correlation between celastrol's apoptotic efficiency and its capacity to enhance intracellular ROS levels, we performed a repeat flow cytometry analysis to assess the levels of ROS in ONS-76 cells (Fig. 3C). Indeed, we observed that the cells treated with celastrol for 24 hrs exhibited significantly elevated levels of ROS in comparison to the control group (Fig. 3D), suggesting that celastrol has the capability to induce apoptosis via upregulation of ROS levels in SHH subtype MB.

Comparative transcriptome analysis investigates the impact of celastrol on SHH subtype medulloblastoma

To comprehensively investigate the regulatory mechanism of celastrol in SHH subtype MB, we carried out transcriptome analysis to compare the differences between celastrol-treated and DMOS-treated ONS-76 cells. In this study, we identified 514 differentially expressed genes (DEGs), comprising 399 significantly upregulated genes and 115 significantly downregulated genes (Fig. 4A, B). We employed the GO database for further annotation of these DEGs, and discovered that they were associated with a comprehensive set of 1984 GO terms, encompassing 1612 biological processes, 156 cellular components, and 216 molecular functions (Fig. 4C). When considering the Log fold change values, the top 30 most significantly expressed genes were primarily enriched in various biological processes and molecular functions, as shown in Fig. 5A. Notably, the DEGs were prominently enriched in functions such as protein tyrosine/threonine phosphatase activity, extracellular matrix constituent secretion, and MAP kinase enrichment, which included tyrosine or serine/threonine phosphatase activity.

Furthermore, we conducted KEGG analysis with a significance threshold of $p < 0.05$ (Fig. 5B). This analysis identified a total of 258 signaling pathways, with the top 18 enriched terms including: vitamin B6 metabolism, rheumatoid arthritis, bladder cancer, TNF signaling pathway, IL-17 signaling pathway, thyroid cancer, NF-κB signaling pathway, basal cell carcinoma, legionellosis, AGE-RAGE signaling pathway in diabetic complications, colorectal cancer, endometrial cancer, one-carbon pool by folate, epithelial cell signaling in helicobacter pylori infection, antifolate resistance, and the p53 signaling pathway (Fig. 6A).

We validated seven genes chosen from the top 18 pathways identified in the KEGG analysis using quantitative polymerase chain reaction (qPCR), as shown in Fig. 6B. The results exhibited consistency with the findings from the transcriptome analysis.

Celastrol inhibits the growth of SHH type medulloblastoma in vivo

Finally, we performed animal experiments to investigate the anti-tumor effect of celastrol on SHH-MB in vivo (Fig. 7A, B). The animals were administered intraperitoneal injection of 2mg/kg/ day or an equal volume of saline after subcutaneous tumor formation using ONS-76 cells. After a treatment period of 20 days, we consistently observed that mice treated with celastrol showed a significant reduction in tumor volume (Fig. 7C, D) throughout the experimental duration and resected tumor weight at day 33 (Fig. 7E, F), as compared to the control group, despite that there was no notable disparity in body weight between the two groups of mice (Fig. 7G).

Discussion

SHH-MB stands as one of the most prevalent malignant pediatric tumors originating in the cerebellum[17]. SHH-MB cells rely on continuous Shh signaling, yet targeted therapies for SHH-MB have faced challenges due to drug resistance[18]. In this study, therefore, we performed a screening of a compound library consisting of inhibitors targeting autophagy and UPS pathways. We found that celastrol can inhibit the proliferation of SHH-MB. In light of this, we identified celastrol, a plant-derived triterpene, which offers significant promise for MB treatment.

Celastrol, a natural compound derived from the traditional Chinese medicinal herb Tripterygium wilfordii Hook F, boasts a wide range of pharmacological properties[19]. This versatile compound exhibits potent pharmacological activity, delivering pronounced anti-cancer, anti-tumor and anti-diabetes effects[20]. It is well-documented that celastrol possesses the capability to influence a wide array of signaling pathways[21]. Celastrol, being a unique compound, exerts the ability to modulate both autophagy and apoptosis, and it triggers mitochondrial biogenesis through the upregulation of AMPK and sirtuin 1 (SIRT1) signaling pathways[22]. In breast cancer cells, celastrol possesses the capability to induce the ubiquitin-dependent degradation of mTOR[23]. Furthermore, celastrol-induced autophagy and apoptosis are contingent upon the deactivation of the PI3K/Akt/mTOR signaling pathway and ROS-mediated mitochondrial dysfunction[24]. Additionally, it has been reported that celastrol can modulate the expression of pro-inflammatory cytokines, MHC II, HO-1, iNOS, NF-κB, Notch-1, CXCR4, TRAIL receptors DR4 and DR5, CHOP, JNK, VEGF, adhesion molecules, proteasome activity, topoisomerase II, potassium channels, and the heat shock response[25]. Our present study demonstrates that celastrol exhibits potent anticancer effects in MB both in vitro and in vivo by inhibiting cell proliferation, migration, and invasion. Notably, celastrol achieves its anti-proliferative effects by modulating intracellular ROS levels and inducing apoptosis. Recent research has unveiled novel functions of the MEK/MAPK pathway in the regulation of human SHH-MB tumorigenesis[26]. Importantly, we found that celastrol primarily inhibits the proliferation, migration, and invasion of MB through the MAPK signaling pathway, NF-κB signaling pathway, TNF signaling pathway, and IL-17 signaling pathway.

Apoptosis, a programmed cell death process, plays a pivotal role in cancer therapy[27]. Celastrol exerts its cytotoxic effects by inducing cell cycle arrest at the G2/M phase and activating both intrinsic and extrinsic apoptotic pathways[28]. Extensive research has previously demonstrated that celastrol possesses potent antitumor effects on a variety of cancer cells by targeting the AKT/mTOR signaling

pathway[29]. Celastrol elevates intracellular ROS levels, leading to ROS-dependent endoplasmic reticulum stress, mitochondrial dysfunction, and ultimately apoptosis[30]. Additionally, celastrol induces apoptosis by promoting the accumulation of mitochondrial ROS to inhibit the STAT3 pathway in non-small cell lung cancer[31]. STAT3 activity, in turn, represses p21 expression and fosters the formation of colonies in SHH-MB cells. However, the combined treatment with inhibitors targeting both Smo and STAT3 leads to a marked synergistic effect, effectively overcoming drug resistance in Smo antagonist-resistant SHH-MB cells[32]. Our current study further establishes that celastrol induces apoptosis in ONS-76 cells, with notable increases in ROS levels following celastrol treatment. At the transcriptome level, it's plausible that celastrol's induction of apoptosis occurs through modulation of the AKT/mTOR signaling and STAT3 pathway.

Proliferation, a hallmark of cancer, plays a pivotal role in tumor treatment strategies[33]. Celastrol, for example, exhibits its therapeutic potential by effectively restraining laser-induced choroidal neovascularization, primarily through the suppression of VEGF-induced proliferation[34]. The p53 network, a critical tumor-suppressive mechanism, orchestrates the transcriptional activation of target genes to counteract excessive cellular proliferation in various human malignancies[35]. Our research findings suggest that celastrol may exert its anti-proliferative effects on MB cells by modulating both the VEGF pathway and the p53 pathway.

Tumor invasion and metastasis are intrinsically linked to the process of epithelial-to-mesenchymal transition (EMT)[36]. EMT represents a reversible cellular program that transforms epithelial cells into mesenchymal states characterized by enhanced motility and invasive properties[37]. Notably, VEGF assumes a crucial role in regulating the metastatic behavior of NPC cells by modulating EMT markers and MMPs in an autocrine manner[38]. Similarly, TNF-alpha influences the role of EMT in facilitating invasion and metastasis in oral squamous carcinoma cells through the MAPK signaling pathway[39]. Moreover, the ability of celastrol to inhibit EMT extends to its impact on other signaling pathways, including SIRT1, NFAT1, SMAD, IL-6, STAT3, AQP5, Notch 1, PI3K/Akt, Wnt/beta-catenin, NF-κB, FAK/AKT, and Hedgehog (Hh)[40]. These findings align with our research, indicating that celastrol effectively impedes the migration and invasion of ONS76 cells. This effect is likely mediated by the suppression of EMT activity, influenced by the interplay of VEGF, TNF-alpha, NF-κB, and the MAPK signaling pathway.

Our study demonstrated that celastrol effectively suppressed the proliferation, migration, and invasion of SHH-MB cells while promoting apoptosis. To assess the viability of celastrol as an anticancer drug, we established a MB xenograft mouse model and administered celastrol. Encouragingly, celastrol efficiently inhibited MB growth without exerting a significant impact on the mice's overall growth. These results underscore the potential of celastrol as a promising chemotherapeutic agent for the treatment of SHH-MB.

In conclusion, the identification of celastrol and its potential mechanisms of MB suppression offer a promising avenue in the realm of pediatric oncology. To fully assess its therapeutic capabilities in the context of MB, additional research, spanning preclinical and clinical investigations, is imperative. Should

these efforts yield success, celastrol may emerge as a substantial contributor to the enhancement of treatment strategies for this devastating form of cancer.

Methods

Chemicals

The library of ubiquitinated and autophagic compounds was purchased from TargetMol (United States). Celastrol was obtained from TargetMol (Cat# 34157-83-0, United States). Fetal calf serum (FCS) was sourced from LONSERA (Cat# S711-001S, Uruguay). DMEM (Cat# 11995-065), penicillin–streptomycin (Cat# 10378016), and 0.25% Trypsin-EDTA (Cat# 25200-072) were procured from Gibco (United States). DPBS (Cat# 14190144, China) was obtained from ThermoFisher. The CCK-8 kit was sourced from NCM Biotech (Cat# c6005, China). Matrigel was sourced from Corning (Cat#356234, United States). The Reactive Oxygen Species Assay Kit was sourced from Yeasen (Cat# 50101ES01, China). HiScript II Q RT SuperMix for qPCR (Cat# R223-01, China) and ChamQ Universal SYBR qPCR Master Mix (Cat# Q711-03, China) were obtained from Vazyme.

Cell culture

The ONS-76 cell lines were acquired from the Japanese Collection of Research Bioresources Cell Bank (Cat#IFO50355, Japan) and cultured in DMEM containing 10% FCS and 1% penicillin–streptomycin. The cells were cultured at 37°C with 5% CO_2 in a humidified environment.

Drug screening assay

The ONS-76 seeded in a 96-well plate (5000 cells per well) was treated with each drug from the library at a final concentration of 10μM for 48 hours (hrs). CCK8 reagent was then added, and the OD450 value was measured following a 1-hr incubation at 37°C. DMSO-treated cells were served as negative control.

Assessment of the 50% inhibitory concentration of celastrol

The ONS-76 seeded in a 96-well plate (5000 cells per well), treated with celastrol at concentrations ranging from 0 to 64 μM, and then incubated for 24 hrs. CCK8 reagent was then added, and the OD450 value was measured following a 1-hr incubation at 37°C. Each experiment had three accessory Wells, and each experiment was repeated at least three times. Data analysis was analyzed using the GraphPad Prism.

Clonogenic proliferation assay

ONS-76 cells were trypsinized, and 200 viable cells were plated in 6-well plates. Following 5 days, the cells were subjected to treatment with celastrol at a concentration of 0 or 1 μM. Another 5 days later, the cells

were fixed and stained with 0.5% crystal violet (Sigma-Aldrich, St. Louis, MO, United States), and the visible colonies were subsequently counted.

Wound healing assay

Cells were seeded in 6-well plates at a density of 5×10^5 cells per well and incubated overnight at 37°C with 5% CO_2. The cell monolayers were scratched vertically using a pipette tip and then subjected to three PBS washes. In the control group, serum-free DMEM was added, while in the celastrol group, 2 μM celastrol was added. The plates were returned to the incubator, and images were taken at a consistent field of view for each group at 0, 12, 24, and 48 hours. The extent of healing between the scratch lines was quantified using ImageJ software (v2.9.0).

Cell migration and invasion assay

For the cell migration assay, cells were resuspended in serum-free DMEM at a concentration of 5×10^5 cells/ml. In the control group, 100 μl of the cell suspension was combined with 100 μl of DMEM, while in the celastrol group, 100 μl of the cell suspension was mixed with 100 μl of 4 μM celastrol and added to the upper chamber. Simultaneously, 600 μl of complete medium (medium containing 10% FCS) was introduced into the lower chamber. After 6 hours of incubation, the upper chamber was fixed with 4% paraformaldehyde for 15 min, and subsequently stained with 0.5% crystal violet for additional 15 min.

For the invasion assay, 0.2% Matrigel was introduced into the upper chamber before cell seeding. Cells were resuspended in serum-free DMEM at a concentration of 6×10^5 cells/ml. In the control group, 100 μl of the cell suspension was mixed with 100 μl of DMEM, while in the celastrol group, 100 μl of the cell suspension was combined with 100 μl of 4 μM celastrol and added to the upper chamber. Simultaneously, 600 μl of complete medium (containing 10% FCS) was introduced into the lower chamber. The culture duration was extended to 24 hours. Images were captured using a Zeiss microscope (Germany) after the chambers had been dried, and cell counts were quantified using Fiji software (v2.9.0).

Flow cytometry

ONS-76 cells were seeded into a 6-well plate (1×10^6 cells/well) and treated separately with celastrol at a final concentration of 2.1 μM for 24 hrs.

In the detection of ROS, we utilized the ROS assay kit. Cells were rinsed with DPBS two times, diluted in DMEM at a 1:1000 ratio, and incubated in a light-protected cell culture incubator at 37°C for 30 min.

In the detection of apoptosis, we used the Annexin V-fluorescein isothiocyanate (FITC) kit (Beyotime Institute of Biotechnology). Cells were rinsed with DPBS two times, collected and resuspended in a binding buffer and stained with Annexin V-FITC/propidium iodide (PI). Cell apoptosis was examined by flow cytometry (Thermo Fisher Scientific, Waltham, MA, United States).

Data analysis was analyzed using the FlowJo software (Tree Star Inc, Ashland, OR).

RNA Sequencing Technique

ONS-76 cells were seeded in a 6-well plate with a density of 4×10^5 cells per well. The three biological samples were then treated with celastrol at a concentration of 2.1 μM for 24 hrs, while another three samples were treated with DMSO for 24 hrs. The six biological samples were collected using TRIzol Reagent. The six biological samples were subsequently transported to the Sinotech Genomics Co., Ltd (Shanghai, China). Total RNA was isolated using RNeasy mini kit (Qiagen, Germany), after which the RNA concentration and quality were determined by the Qubit®3.0 Fluorometer (Life Technologies, USA) and the Nanodrop One spectrophotometer (Thermo Fisher Scientific Inc., USA). Integrity of total RNA was assessed using the Agilent 2100 Bioanalyzer (Agilent Technologies Inc., USA), and samples with RNA integrity number (RIN) values above 7.0 were used for sequencing. One micrograms of RNA were used as input material for the RNA sample preparations.

Paired-end libraries were synthesized by using the Stranded mRNA-seq Lib Prep Kit for lllumina (ABclonal, China) following Preparation Guide. Briefly, the poly-A containing mRNA molecules were purified using poly-T oligo-attached magnetic beads. Following purification, the mRNA is fragmented into small pieces using divalent cations under 94°C for 10 min. The cleaved RNA fragments are copied into first strand cDNA using reverse transcriptase and random primers. This is followed by second strand cDNA synthesis using DNA Polymerase I and RNase H. These cDNA fragments then go through an end repair process, the addition of a single 'A' base, and then ligation of the adapters. The products are then purified and enriched with PCR to create the final cDNA library. Purified libraries were quantified by Qubit® 3.0 Fluorometer (Life Technologies, USA) and validated by Agilent 2100 bioanalyzer (Agilent Technologies, USA) to confirm the insert size and calculate the mole concentration. Cluster was generated by cBot with the library diluted to 10 pM and then were sequenced on the Illumina NovaSeq 6000 (Illumina, USA).

Quantitative PCR

ONS-76 cells were seeded in a 6-well plate at a density of 4×10^5 cells per well. Subsequently, they were treated with Celastrol at a concentration of 2 μM for 24 hrs. Total cellular RNA was isolated using TRIzol reagent (Invitrogen) as per the manufacturer's instructions. The total RNA extracted was processed following the established protocol. Reverse transcription into cDNA was carried out using HiScript Q RT SuperMix. Real-time PCR was then conducted using ChamQ Universal SYBR qPCR Master Mix, with triplicate samples run on a Bio-Rad(CFX Opus)qPCR system in accordance with the manufacturer's instructions. Ct values were normalized to GAPDH, and quantitative analysis was conducted using the $2^{-\Delta\Delta Ct}$ method. The sequences of the primers used are listed in table1.

Tumor xenografts in nude mice

ONS-76 cells (5×10^6) were suspended in PBS and injected subcutaneously into 6-week-old BALB/c nude mice (Shanghai Laboratory Animal Center, Shanghai, China). About 14 days later, the mice were randomly divided into two groups: a control group and a celastrol group. The control group of mice received a daily oral administration of 300 μL of saline, while the celastrol group was given a daily oral dose of 300 μL of

celastrol at 2 mg/kg/daily. The mice were measured for body weight and tumor volume every 2 days. The tumor volumes were measured using a vernier caliper and calculated as 0.5 × length × width^2. After 20 days of treatment, the tumors were excised from the mice, weighed, and photographed.

Statistical analysis

Statistical analysis was conducted using GraphPad Prism 9.5.1 (GraphPad Software, Version X; La Jolla, CA, United States). All experimental data were displayed as mean ± standard deviation. Statistical analysis of the data was carried out using *unpaired* t test, one-way analysis of variance (ANOVA), or two-way ANOVA. A significance level of $p < 0.05$ was used to determine statistical significance.

Declarations

Statement of ethics

Protocols of animal care and use complied with the Regulations for the Administration of Affairs Concerning Experimental Animals approved by the State Council of the People's Republic of China. Animal Ethical and Experimental Committee of Wenzhou Medical University approve the animal experiment (No. wydw2023-0595).

Data availability

Source data supporting the findings of the present study are included in the article. The transcriptome of celastrol treatment group and blank control group was deposited in NCBI under BioProject PRJNA1022993.

Funding

The present study is supported by the Second Affiliated Hospital and Yuying Children's Hospital of Wenzhou Medical University Doctoral Research Foundation (No. ZXCVBNM00001514, China).

CRediT authorship contribution statement

Bohong Wang: Conceptualization, Methodology, Validation, Formal analysis, Investigation, Data curation, Writing – original draft, Visualization, Supervision, **Tao Xu:** Conceptualization, Methodology, Validation, Data curation, **Lisheng Yu:** Conceptualization, Methodology, **Chenjie Qiu:** Conceptualization, Methodology, **Chao Xu:** Methodology, Data Curation, **Xiangmao Zhao:** Methodology, Data Curation, **Shangyu Xu:** Methodology, **Hansong Sheng:** Resources, Writing – original draft, Writing –review & editing, **Feng Tan:** Resources, Writing – original draft, Writing –review & editing, Supervision, Project administration, Funding acquisition, **Nu Zhang:** Conceptualization, Methodology, Validation, Formal analysis, Investigation, Resources, Writing – original draft, Writing –review & editing, Supervision, Project administration, Funding acquisition.

Declaration of Competing Interest

The authors declare that they have no known competing financial interests or personal relationships that could have appeared to influence the work reported in this paper.

Acknowledgements

We thank Wenzhou Key Laboratory of Neurodevelopmental Pathology and Physiology for providing the venue and support for this experiment.

References

1. Martinez de Estibariz I, Jakjimovska A, Illarregi U, Martin-Guerrero I, Gutierrez-Camino A, Lopez-Lopez E, Bilbao-Aldaiturriaga N: **The Role of the Dysregulation of Long Non-Coding and Circular RNA Expression in Medulloblastoma: A Systematic Review.** *Cancers (Basel)* 2023, **15**.
2. Jaruthien T, Nantavithya C, Santisukwongchote S, Shuangshoti S, Techavichit P, Sosothikul D, Amornfa J, Shotelersuk K: **Postoperative radiotherapy timing, molecular subgroups and treatment outcomes of Thai pediatric patients with medulloblastoma.** *PLoS One* 2023, **18:**e0271778.
3. Ciobanu-Caraus O, Czech T, Peyrl A, Haberler C, Kasprian G, Furtner J, Kool M, Sill M, Frischer JM, Cho A, et al: **The Site of Origin of Medulloblastoma: Surgical Observations Correlated to Molecular Groups.** *Cancers (Basel)* 2023, **15**.
4. Strejczek A, Woszczyk D, Urbaniak H, Rozanska M, Robak M, Matuszewska Z, Barciszewska AM: **Epigenetic-Based Therapy-A Prospective Chance for Medulloblastoma Patients' Recovery.** *Int J Mol Sci* 2021, **22**.
5. Marchetti L, Novelli F, Tanno B, Leonardi S, Hizam VM, Arcangeli C, Santi L, Baschieri S, Lico C, Mancuso M: **Peptide-Functionalized and Drug-Loaded Tomato Bushy Stunt Virus Nanoparticles Counteract Tumor Growth in a Mouse Model of Shh-Dependent Medulloblastoma.** *Int J Mol Sci* 2023, **24**.
6. Skowron P, Farooq H, Cavalli FMG, Morrissy AS, Ly M, Hendrikse LD, Wang EY, Djambazian H, Zhu H, Mungall KL, et al: **The transcriptional landscape of Shh medulloblastoma.** *Nat Commun* 2021, **12:**1749.
7. Caimano M, Lospinoso Severini L, Loricchio E, Infante P, Di Marcotullio L: **Drug Delivery Systems for Hedgehog Inhibitors in the Treatment of SHH-Medulloblastoma.** *Front Chem* 2021, **9:**688108.
8. Lospinoso Severini L, Ghirga F, Bufalieri F, Quaglio D, Infante P, Di Marcotullio L: **The SHH/GLI signaling pathway: a therapeutic target for medulloblastoma.** *Expert Opin Ther Targets* 2020, **24:**1159-1181.
9. Hama Y, Ogasawara Y, Noda NN: **Autophagy and cancer: Basic mechanisms and inhibitor development.** *Cancer Sci* 2023, **114:**2699-2708.
10. Garcia-Perez BE, Perez-Torres C, Baltierra-Uribe SL, Castillo-Cruz J, Castrejon-Jimenez NS: **Autophagy as a Target for Non-Immune Intrinsic Functions of Programmed Cell Death-Ligand 1 in Cancer.** *Int J*

Mol Sci 2023, **24**.

11. Booth L, Roberts JL, Poklepovic A, Dent P: **Autophagy as a therapeutic mechanism to kill drug-resistant cancer cells.** *Anticancer Drugs* 2023.
12. Li Y, Chen Y: **AMPK and Autophagy.** *Adv Exp Med Biol* 2019, **1206:**85-108.
13. Keerthana CK, Rayginia TP, Shifana SC, Anto NP, Kalimuthu K, Isakov N, Anto RJ: **The role of AMPK in cancer metabolism and its impact on the immunomodulation of the tumor microenvironment.** *Front Immunol* 2023, **14:**1114582.
14. Yuan W, Fang W, Zhang R, Lyu H, Xiao S, Guo D, Ali DW, Michalak M, Chen XZ, Zhou C, Tang J: **Therapeutic strategies targeting AMPK-dependent autophagy in cancer cells.** *Biochim Biophys Acta Mol Cell Res* 2023, **1870:**119537.
15. Yang W, Wang S, Tong S, Zhang WD, Qin JJ: **Expanding the ubiquitin code in pancreatic cancer.** *Biochim Biophys Acta Mol Basis Dis* 2023, **1870:**166884.
16. LaPlante G, Zhang W: **Targeting the Ubiquitin-Proteasome System for Cancer Therapeutics by Small-Molecule Inhibitors.** *Cancers (Basel)* 2021, **13**.
17. Zhang ZW, Teng X, Zhao F, Ma C, Zhang J, Xiao LF, Wang Y, Chang M, Tian Y, Li C, et al: **METTL3 regulates m(6)A methylation of PTCH1 and GLI2 in Sonic hedgehog signaling to promote tumor progression in SHH-medulloblastoma.** *Cell Rep* 2022, **41:**111530.
18. Borlase S, DeCarlo A, Coudiere-Morrison L, Liang L, Porter CJ, Ramaswamy V, Werbowetski-Ogilvie TE: **Cross-species analysis of SHH medulloblastoma models reveals significant inhibitory effects of trametinib on tumor progression.** *Cell Death Discov* 2023, **9:**347.
19. Wang C, Dai S, Zhao X, Zhang Y, Gong L, Fu K, Ma C, Peng C, Li Y: **Celastrol as an emerging anticancer agent: Current status, challenges and therapeutic strategies.** *Biomed Pharmacother* 2023, **163:**114882.
20. Song J, He GN, Dai L: **A comprehensive review on celastrol, triptolide and triptonide: Insights on their pharmacological activity, toxicity, combination therapy, new dosage form and novel drug delivery routes.** *Biomed Pharmacother* 2023, **162:**114705.
21. Zhang C, Wang W, Du C, Li H, Zhou K, Luan Z, Chang Y, Liu S, Wei Y: **Autophagy in the pharmacological activities of celastrol (Review).** *Exp Ther Med* 2023, **25:**268.
22. Abu Bakar MH, Shariff KA, Tan JS, Lee LK: **Celastrol attenuates inflammatory responses in adipose tissues and improves skeletal muscle mitochondrial functions in high fat diet-induced obese rats via upregulation of AMPK/SIRT1 signaling pathways.** *Eur J Pharmacol* 2020, **883:**173371.
23. Li X, Zhu G, Yao X, Wang N, Hu R, Kong Q, Zhou D, Long L, Cai J, Zhou W: **Celastrol induces ubiquitin-dependent degradation of mTOR in breast cancer cells.** *Onco Targets Ther* 2018, **11:**8977-8985.
24. Zhou M, Liao J, Lai W, Xu R, Liu W, Xie D, Wang F, Zhang Z, Huang J, Zhang R, Li G: **A celastrol-based nanodrug with reduced hepatotoxicity for primary and metastatic cancer treatment.** *EBioMedicine* 2023, **94:**104724.

25. Kannaiyan R, Shanmugam MK, Sethi G: **Molecular targets of celastrol derived from Thunder of God Vine: potential role in the treatment of inflammatory disorders and cancer.** *Cancer Lett* 2011, **303:**9-20.
26. Zagozewski J, Borlase S, Guppy BJ, Coudiere-Morrison L, Shahriary GM, Gordon V, Liang L, Cheng S, Porter CJ, Kelley R, et al: **Combined MEK and JAK/STAT3 pathway inhibition effectively decreases SHH medulloblastoma tumor progression.** *Commun Biol* 2022, **5:**697.
27. Banasavadi-Siddegowda YK, Namagiri S, Otani Y, Sur H, Rivas S, Bryant JP, Shellbourn A, Rock M, Chowdhury A, Lewis CT, et al: **Targeting protein arginine methyltransferase 5 sensitizes glioblastoma to trametinib.** *Neurooncol Adv* 2022, **4:**vdac095.
28. Hsieh MJ, Wang CW, Lin JT, Chuang YC, Hsi YT, Lo YS, Lin CC, Chen MK: **Celastrol, a plant-derived triterpene, induces cisplatin-resistance nasopharyngeal carcinoma cancer cell apoptosis though ERK1/2 and p38 MAPK signaling pathway.** *Phytomedicine* 2019, **58:**152805.
29. Cai Z, Qian B, Pang J, Tan ZB, Zhao K, Lei T: **Celastrol Induces Apoptosis and Autophagy via the AKT/mTOR Signaling Pathway in the Pituitary ACTH-secreting Adenoma Cells.** *Curr Med Sci* 2022, **42:**387-396.
30. Chen X, Zhao Y, Luo W, Chen S, Lin F, Zhang X, Fan S, Shen X, Wang Y, Liang G: **Celastrol induces ROS-mediated apoptosis via directly targeting peroxiredoxin-2 in gastric cancer cells.** *Theranostics* 2020, **10:**10290-10308.
31. Zhao Z, Wang Y, Gong Y, Wang X, Zhang L, Zhao H, Li J, Zhu J, Huang X, Zhao C, et al: **Celastrol elicits antitumor effects by inhibiting the STAT3 pathway through ROS accumulation in non-small cell lung cancer.** *J Transl Med* 2022, **20:**525.
32. Yuan L, Zhang H, Liu J, Malhotra A, Dey A, Yu B, Jella KK, McSwain LF, Schniederjan MJ, MacDonald TJ: **STAT3 is required for Smo-dependent signaling and mediates Smo-targeted treatment resistance and tumorigenesis in Shh medulloblastoma.** *Mol Oncol* 2022, **16:**1009-1025.
33. Hashemi M, Hasani S, Hajimazdarany S, Mirmazloomi SR, Makvandy S, Zabihi A, Goldoost Y, Gholinia N, Kakavand A, Tavakolpournegari A, et al: **Non-coding RNAs targeting notch signaling pathway in cancer: From proliferation to cancer therapy resistance.** *Int J Biol Macromol* 2022, **222:**1151-1167.
34. Li Z, Zhou KW, Chen F, Shang F, Wu MX: **Celastrol inhibits laser-induced choroidal neovascularization by decreasing VEGF induced proliferation and migration.** *Int J Ophthalmol* 2022, **15:**1221-1230.
35. Yang K, Xiao Y, Zhong L, Zhang W, Wang P, Ren Y, Shi L: **p53-regulated lncRNAs in cancers: from proliferation and metastasis to therapy.** *Cancer Gene Ther* 2023.
36. Saitoh M: **Transcriptional regulation of EMT transcription factors in cancer.** *Semin Cancer Biol* 2023.
37. Zhong BH, Dong M: **The implication of ciliary signaling pathways for epithelial-mesenchymal transition.** *Mol Cell Biochem* 2023.
38. Chen L, Lin G, Chen K, Liang R, Wan F, Zhang C, Tian G, Zhu X: **VEGF promotes migration and invasion by regulating EMT and MMPs in nasopharyngeal carcinoma.** *J Cancer* 2020, **11:**7291-7301.

39. Zhao XW, Zhou JP, Bi YL, Wang JY, Yu R, Deng C, Wang WK, Li XZ, Huang R, Zhang J, Tao DT: **The role of MAPK signaling pathway in formation of EMT in oral squamous carcinoma cells induced by TNF-alpha.** *Mol Biol Rep* 2019, **46:**3149-3156.

40. Avila-Carrasco L, Majano P, Sanchez-Tomero JA, Selgas R, Lopez-Cabrera M, Aguilera A, Gonzalez Mateo G: **Natural Plants Compounds as Modulators of Epithelial-to-Mesenchymal Transition.** *Front Pharmacol* 2019, **10:**715.

Table 1

Table 1 is available in the Supplementary Files section.

Figures

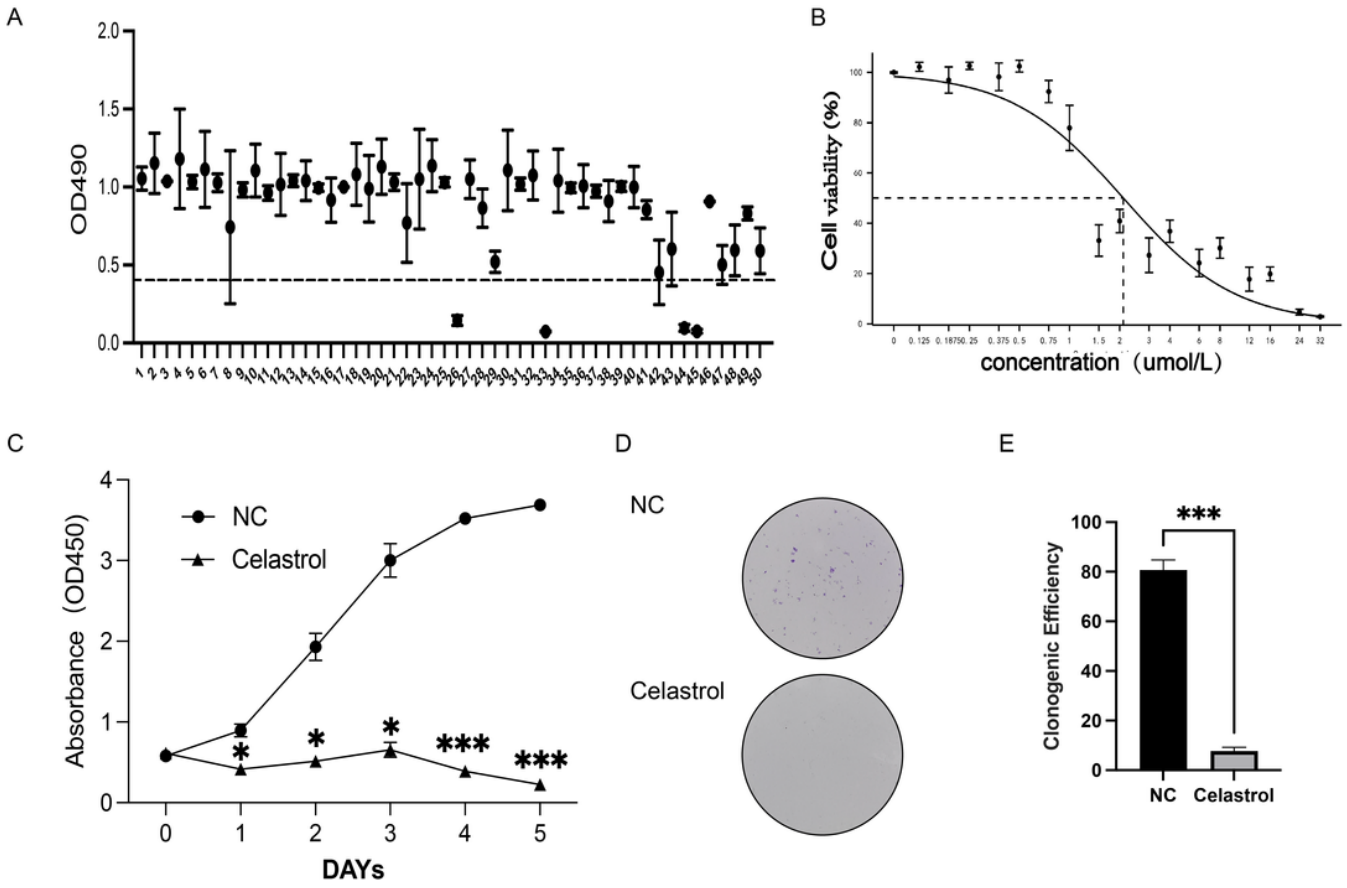


Figure 1. Celastrol inhibited the proliferation of ONS-76 cells. (A) 50 protease inhibitors acting on ONS-76 at a concentration of 10 μM. Data are presented as the mean ± SD, unpaired t test were used to determine the significance.
(B) The IC50 value of celastrol. Data are presented as the mean ± SD, unpaired t test were used to determine the significance.
(C) CCK8 assays for the growth of ONS-76 cells in celastrol and DMSO. Data are presented as the mean ± SD, two-way ANOVA multiple comparisons were used to determine the significance.
(D, E) Colony formation assay was used to detected the effects of celastrol treatment on clone ability of cells(n=3). Data are presented as the mean ± SD, unpaired t test were used to determine the significance.
*p < 0.05; **p < 0.01; ***p < 0.001 compared with the control group.

Figure 1

See image above for figure legend

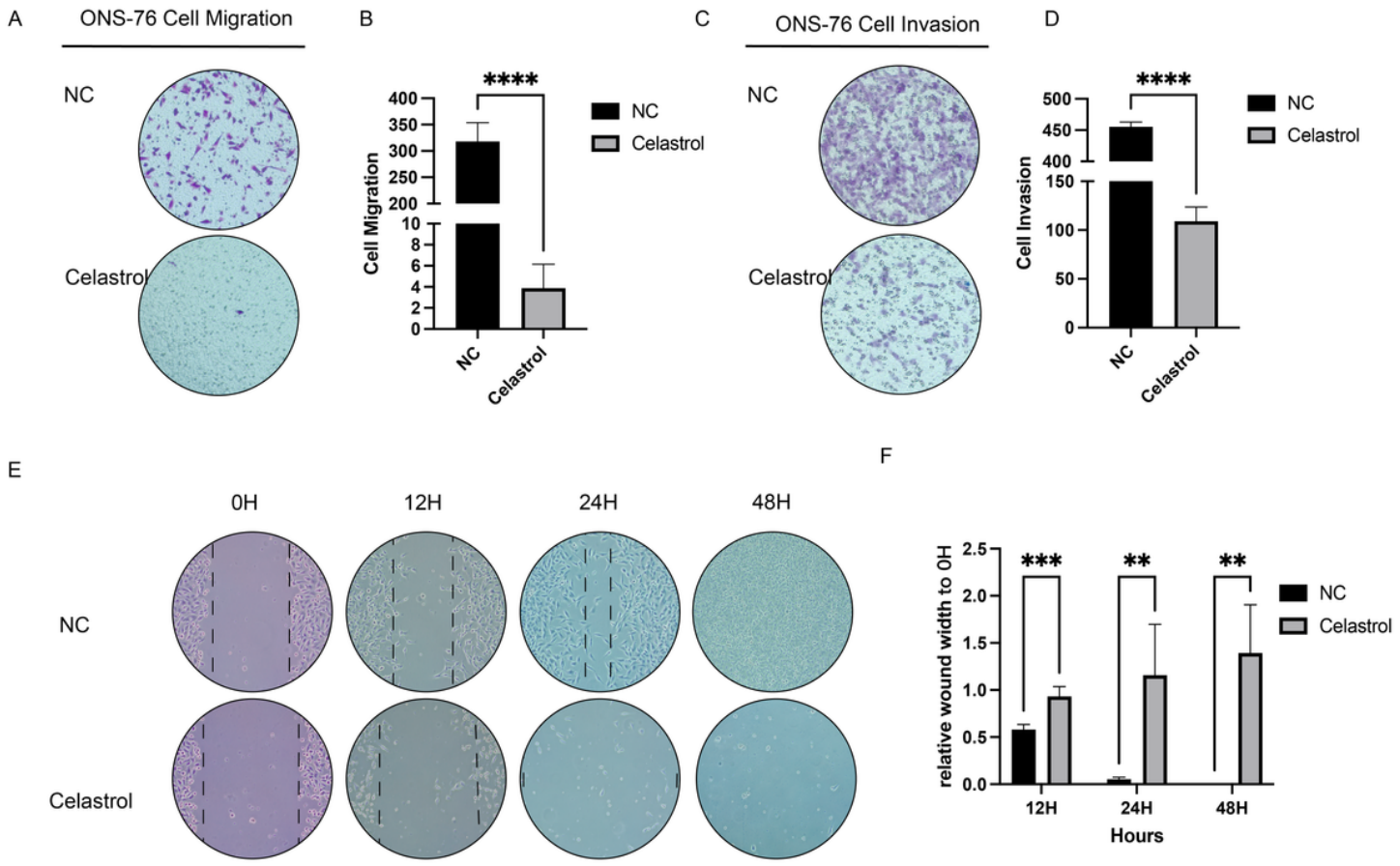


Figure 2. Celastrol suppressed the migration and invasion of ONS-76 cells.
(A, B) Transwell assay was used to assess the migration ability of ONS-76 cells after 6 h of Celastrol treatment (n = 9). Data are presented as the mean ± SD, unpaired t test were used to determine the significance.
(C, D) Transwell assay was used to assess the invasion ability of ONS-76 cells after 24 h of Celastrol treatment (n = 9). Data are presented as the mean ± SD, unpaired t test were used to determine the significance.
(E, F) Scratch assay was used to assess the migration ability of ONS-76 cells after Celastrol treatment (n=6). Data are presented as the mean ± SD, two-way ANOVA multiple comparisons were used to determine the significance.
*p < 0.05; **p < 0.01; ***p < 0.001 compared with the control group.

Figure 2

See image above for figure legend

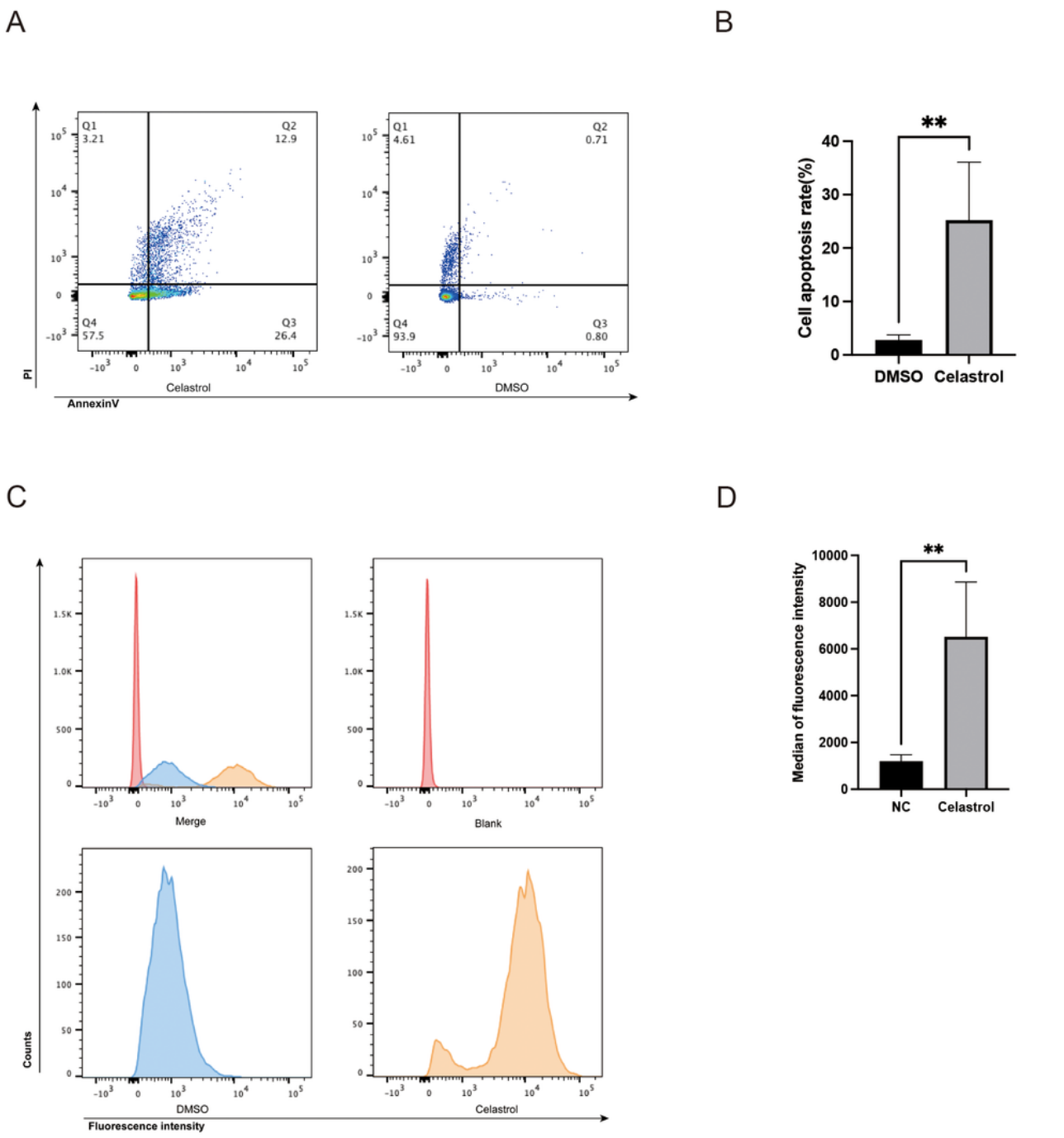


Figure 3. Celastrol can induce cell apoptosis via upregulation of ROS levels.
(A) The flow cytometry of apoptosis in celastrol treatment group versus DMSO group.
(B) Statistical analysis of apoptosis by the flow cytometry. Data are presented as the mean ± SD, unpaired t test were used to determine the significance.
(C) The flow cytometry of ROS in celastrol treatment group versus DMSO group.
(D) Statistical analysis of ROS by the flow cytometry. Data are presented as the mean ± SD, unpaired t test were used to determine the significance.
*p < 0.05; **p < 0.01; ***p < 0.001 compared with the control group.

Figure 3

See image above for figure legend

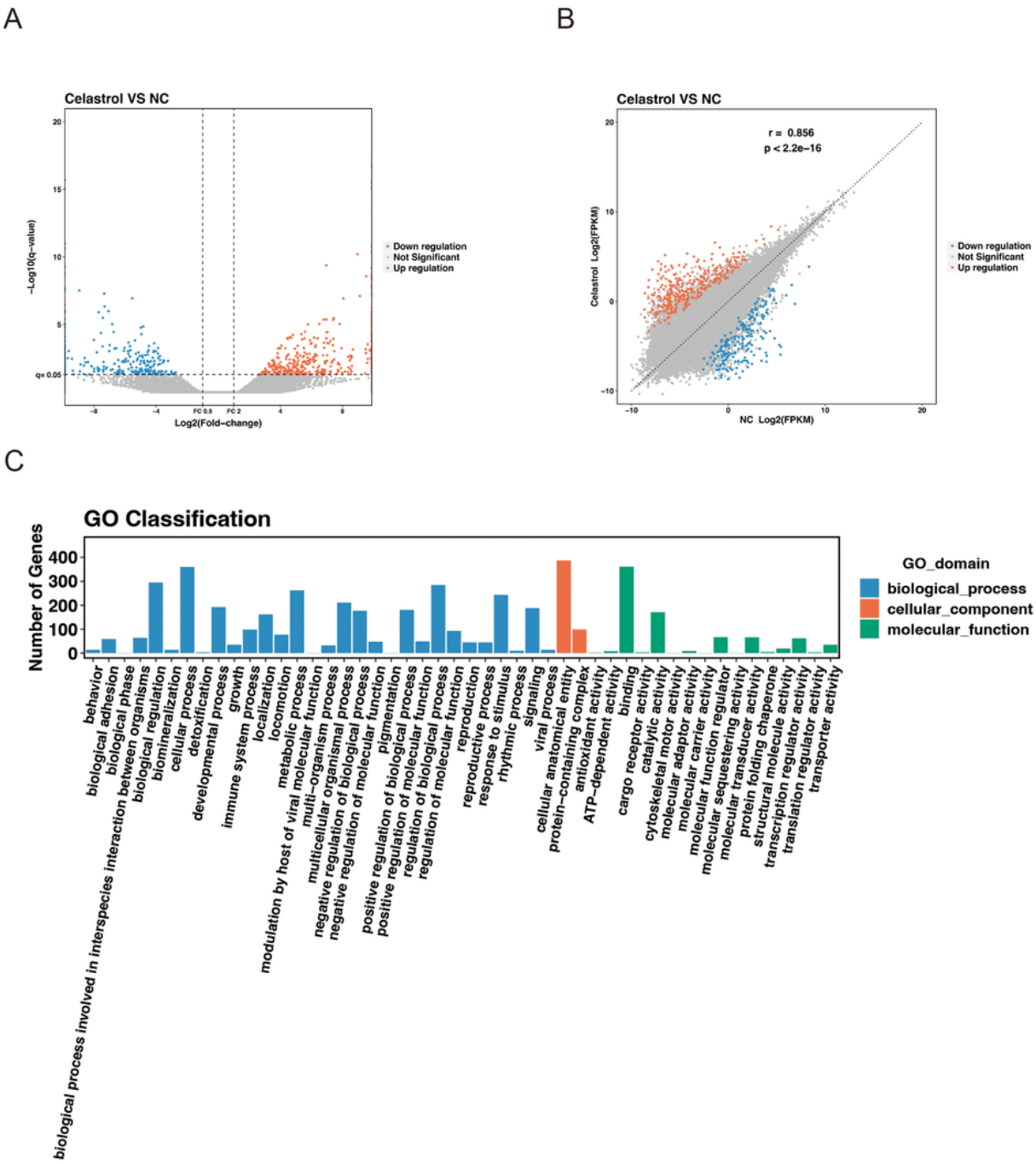


Figure 4. Transcriptome analysis of celastrol and DMSO groups.
(A) Volcano plot of celastrol versus DMSO group.
(B) Scatter plot of the celastrol and DMSO groups.
(C) GO analysis of differentially expressed genes.

Figure 4

See image above for figure legend

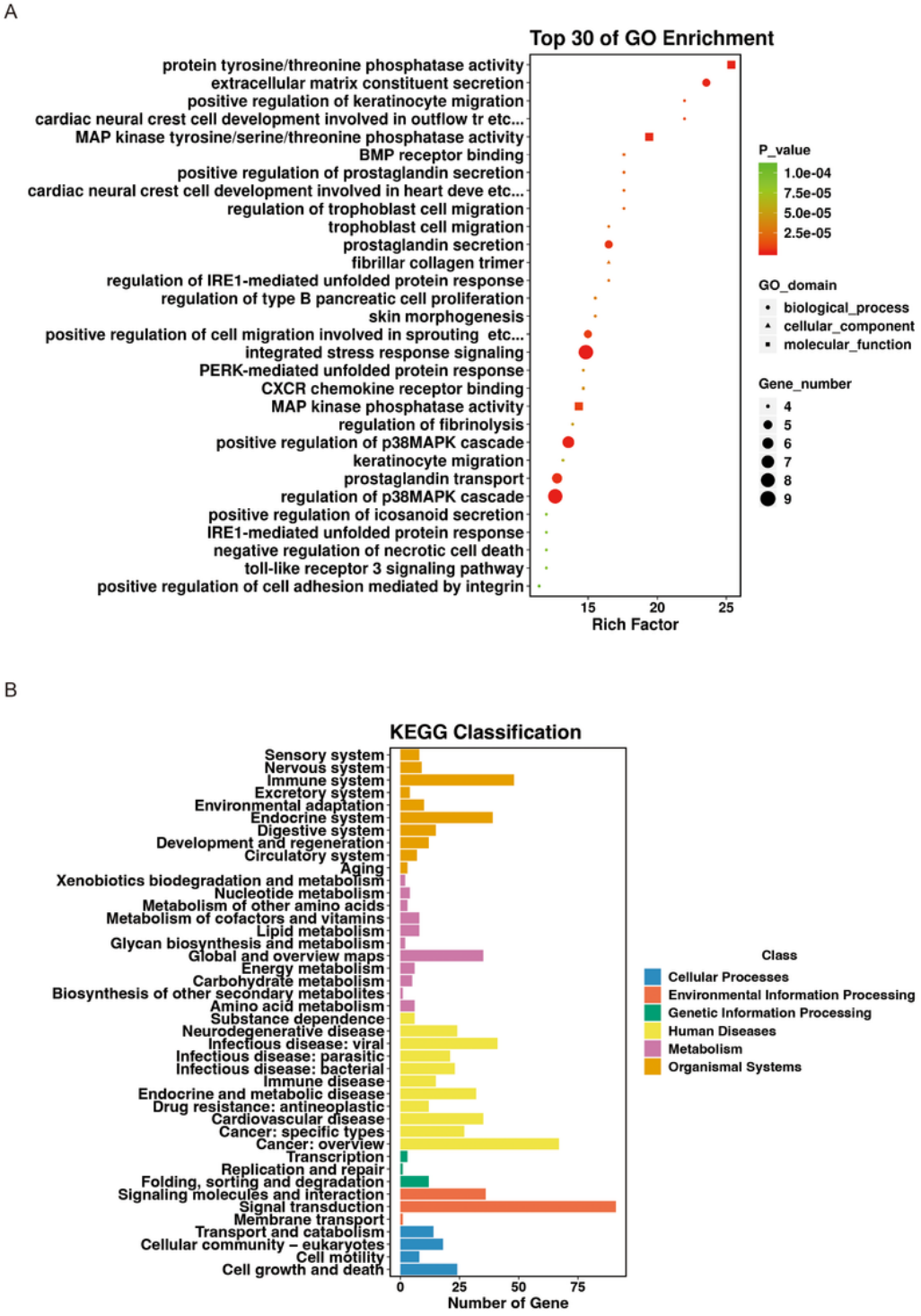
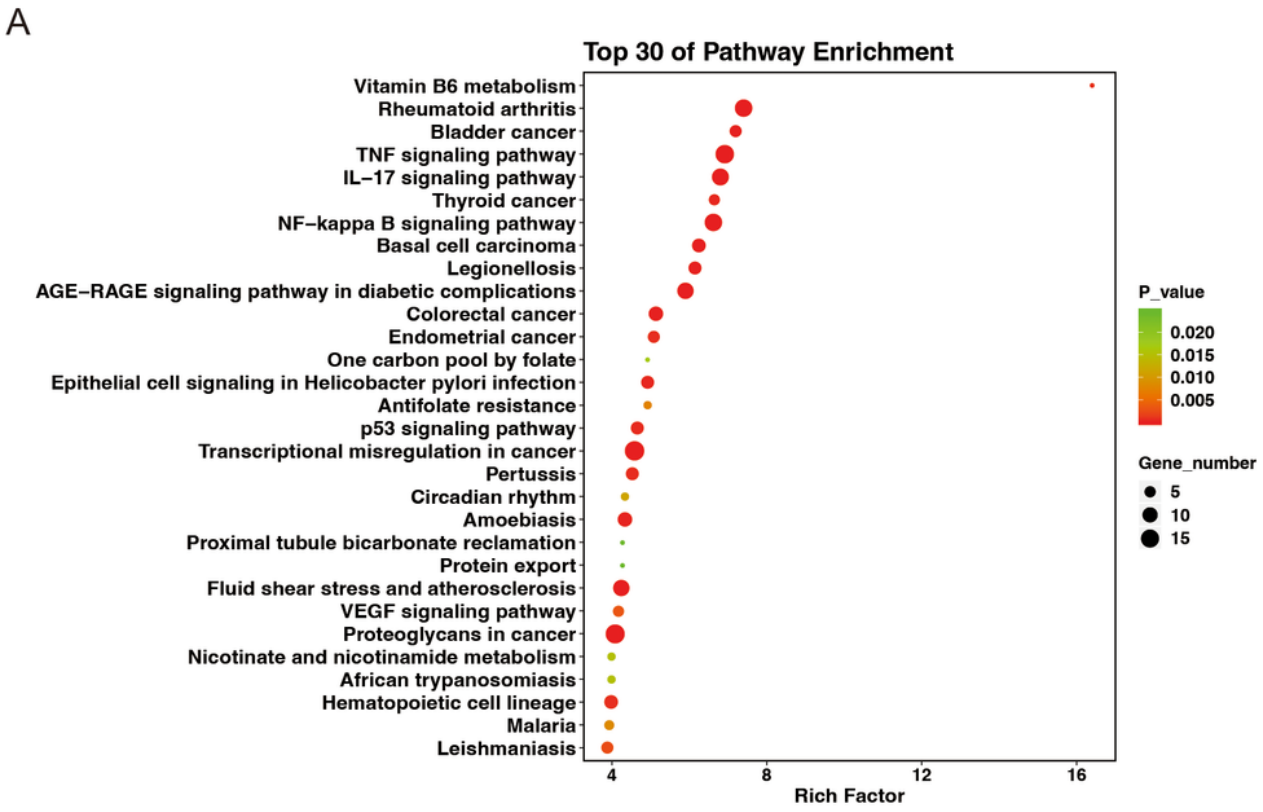


Figure 5. Transcriptome analysis of celastrol and DMSO groups.
(A) GO enrichment analysis of the top 30 most significantly expressed genes.
(B) KEGG analysis of differentially expressed genes.

Figure 5

See image above for figure legend



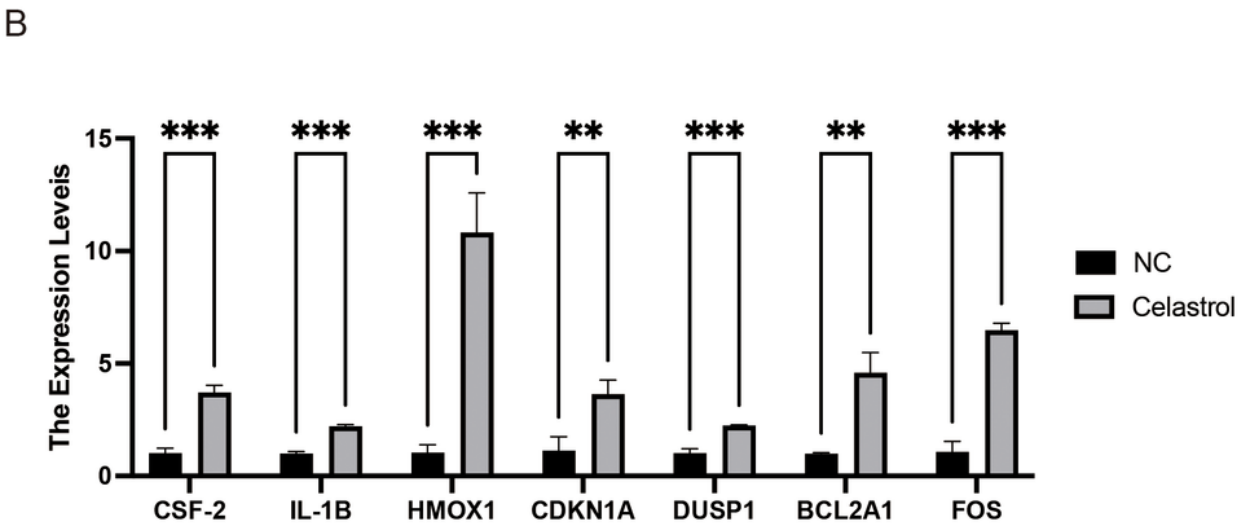


Figure 6. Transcriptome analysis of celastrol and DMSO groups.
(A) KEGG pathway enrichment analysis of the top 30 most significantly expressed genes.
(B) qPCR of celastrol and DMSO groups.
Data are presented as the mean ± SD, two-way ANOVA multiple comparisons, unpaired t test were used to determine the significance.
*p < 0.05; **p < 0.01; ***p < 0.001 compared with the control group.

Figure 6

See image above for figure legend

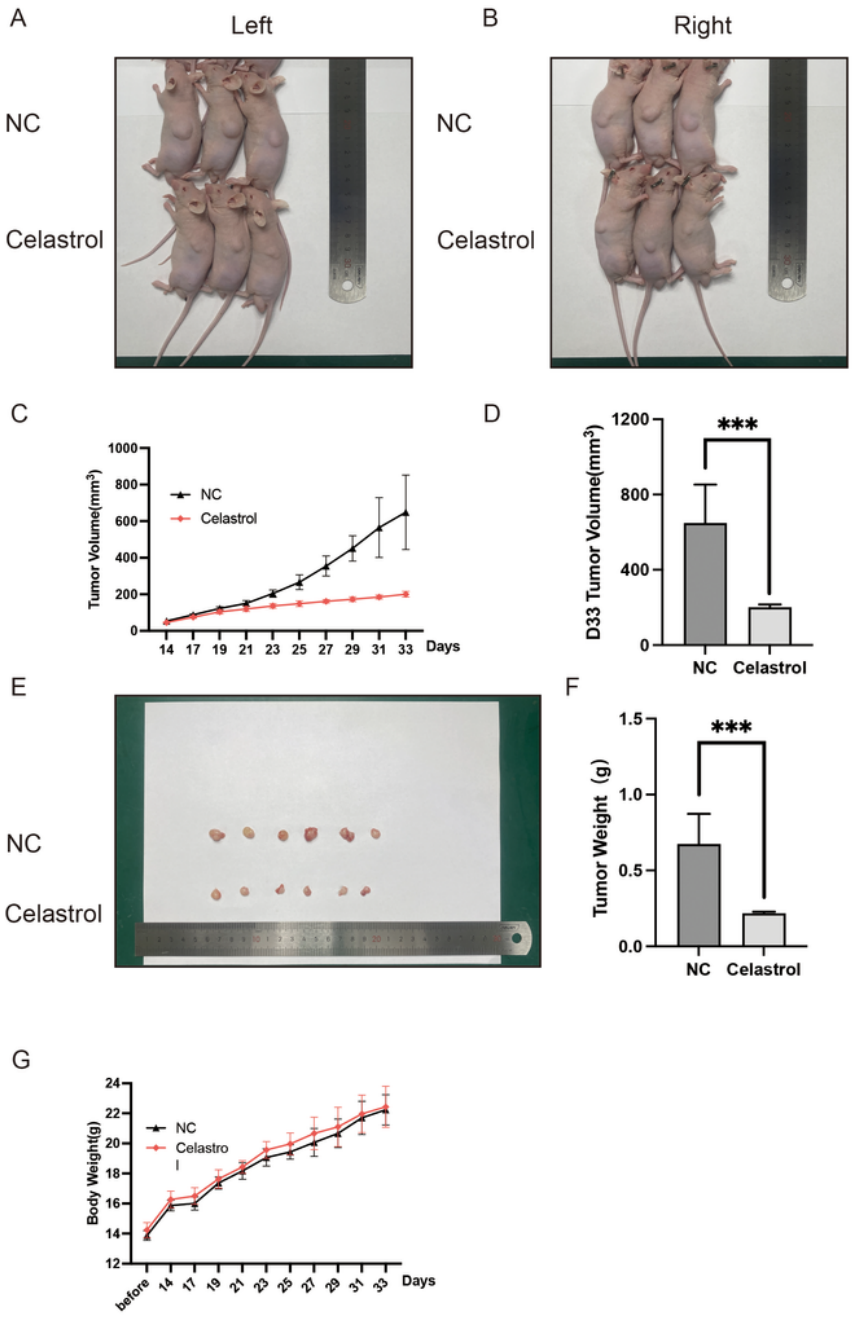


Figure 7. Celastrol inhibits the growth of SHH type medulloblastoma in vivo.
(A, B) Photo of the nude mice bearing subcutaneous xenograft tumor.
(C) Tumor volume was recorded every 2 days. Tumor volume measurement was calculated as: length * width * width *0.5 (mm3).
Data are presented as the mean ± SD, two-way ANOVA multiple comparisons were used to determine the significance.
(D) The volume of the excised tumor tissue. Tumor volume measurement was calculated as: length * width * width *0.5 (mm3).
Data are presented as the mean ± SD, unpaired t test were used to determine the significance.
(E) Photo of tumors removed from mice after 20 days of celastrol (2 mg/kg/day) or saline treatment.
(F) The weight of the excised tumor tissue. (E) Body weight of mice was recorded every 2 days (n = 6).
Data are presented as the mean ± SD, two-way ANOVA multiple comparisons, were used to determine the significance.
*p < 0.05; **p < 0.01; ***p < 0.001 compared with the control group.

Figure 7

See image above for figure legend

Supplementary Files

This is a list of supplementary files associated with this preprint. Click to download.

- table1.xlsx